Supplementary Information

A mild process for producing high-performance dissolving pulp toward highly-substituted cellulose acetate: integrated production of lignin nanoparticles and closed-loop solvent recycling

Xin-Yao Ye [a, b] Xin-Yi Hui [a, b], Qian Sun [a, b], Chen Zhang [a, b], Si Hong [c], Jia-Long Wen [a, b], Tong-Qi Yuan [a, b] *

[a] *State Key Laboratory of Efficient Production of Forest Resources, Beijing Forestry University, Beijing 100083, China*

[b] *Beijing Key Laboratory of Lignocellulosic Chemistry, Beijing Forestry University, Beijing 100083, China*

[c] *College of Chemistry and Materials, Jiangxi Agricultural University, Nanchang 330045, China*

* Corresponding author.

E-mail address: ytq581234@bjfu.edu.cn (T.-Q. Yuan).

1.Experimental section

1.1. Kraft pulping process

Kraft pulping was conducted using a laboratory-scale digester. The liquor-to-wood ratio was maintained at 6:1 (w/w). The cooking conditions included an effective alkali charge of 25% and a sulfidity of 20%, both expressed as Na_2O. The temperature was ramped from room temperature (25 °C) to the maximum temperature (160 °C) over 1 h, followed by a holding time of 2 h at 160 °C. The resulting unbleached chemical pulp was designated as KP-160-2, while the pulp bleached using the same two-stage bleaching procedure was labelled KP-160-2-BP. Kraft lignin was recovered from the black liquor by acidification with hydrochloric acid (pH =2) and labelled as L-KP-160-2.

1.2. Preparation of cellulose acetate (CA) film material

CA films were fabricated by dissolving 10 % CA (w/v) in dichloromethane: methanol (9:1 v/v) solvent mixtures. The mixture was cast onto a borosilicate petri dish and then ambient-dried (24 h, 45 % RH) to obtain homogeneous and transparent films. Commercial CA films were processed under identical formulation parameters for comparative analysis.

1.3. Preparation method of lignin nanoparticles (LNPs)

Following a previous study,[1] L-B/F-130-2 and L-KP-160-2 (1 mg/mL) were dissolved in an acetone/water mixture (4:1, v/v). Lignin nanoparticles were formed by vacuum evaporation at 200 rpm and room temperature until the organic solvent was fully removed, which were marked as R-L.

1.4. Prepared double enzymatic lignin (DEL)

DEL was prepared based on the previous study,[2] bamboo powders were first milled at 450 rpm for 5 h, then 5 g of the ground material was mixed with sodium acetate buffer (pH 4.8) at a 1:20 (g/mL) ratio. Cellulase (Cellic® CTec2, 100 FPU/mL, Novozymes) was added at 35 $FPU \cdot g^{-1}$ of substrate. The mixture was incubated at 50

°C and 150 rpm (ZWYR-2102C, Shanghai, China) for 48 h. Residual carbohydrates were removed by centrifugation (8000 rpm) with sodium acetate buffer (pH 4.8), and the final solid product was obtained by freeze-drying.

1.5. Acetylation of double enzymatic lignin (DEL)

To improve lignin solubility in tetrahydrofuran for the molecular weight determination by the GPC technique, lignin was acetylated. Approximately 30 mg of dry lignin was dissolved in 3 mL of a dimethyl sulfoxide:1-methylimidazole solution (2:1, v/v) and stirred at room temperature in the dark for 12 h. Then, 1 mL of acetic anhydride was added, and the reaction continued for 2 h. The mixture was slowly added to 100 mL of acidified water (pH=2) to precipitate the product, which was collected by centrifugation to obtain the acetylated lignin.

1.6. DES recovery and utilization of recycled waste liquid

The waste liquid obtained after the fourth cycle of DES pulping (R4-WL) was reused for a wood adhesion test. R4-WL was mixed with a 10% (w/w) aqueous solution of polyvinyl alcohol (PVA) at a mass ratio of 1:1. The mixture was stirred at 90 °C for 2 h to obtain the R4-B/F-WL/PVA adhesive. This adhesive was uniformly applied to beech wood boards with an overlap area of 2 ×1 cm for lap-shear testing.

1.7. Analysis procedures

1.7.1. Chemical composition analysis

The chemical compositions were determined using the Laboratory Analytical Procedures (LAP) for biomass from the National Renewable Energy Laboratory (NREL).[3] Briefly, samples were ground into fine powders and dried at 105 °C for 24 h to remove free and some bound water. A 0.30 g portion was treated with 3.0 mL of 72% H_2SO_4 and hydrolyzed in a 30 °C water bath until fully dissolved, then diluted to 4 wt% and further hydrolyzed at 121 °C for 1 h. After cooling to room temperature, samples were filtered for sugar analysis. High-performance anion exchange chromatography (HPAEC, Dionex ICS 3000) was used, equipped with a CarboPac™ PA-20 column (3

× 150 mm), a PA-20 guard column (3 × 30 mm), and an amperometric detector. Each sample was measured in triplicate, and the average was reported to ensure accuracy. The equations used for preprocessing performance analysis (S1–S4) are as follows:

$$\text{Pulp yield}\ (\%) = \frac{\text{Pretreated solid residue}\ (\text{g})}{\text{Raw bamboo}\ (\text{g})} \times 100 \quad \text{(S1)}$$

$$\textit{Delignification ratio}\ (\%) = \left(1 - \frac{\text{Lignin in pretreated solid residue}\ (\text{g})}{\text{Initial amount of lignin in raw bamboo}\ (\text{g})}\right) \times 100 \quad \text{(S2)}$$

$$\text{Lignin recovery ratio}\ (\%) = \frac{\text{Recovered lignin (g)}}{\text{Lignin removed from the feedstock (g)}} \times 100 \quad \text{(S3)}$$

$$\text{Hemicelluloses removal ratio}\ (\%) = \left(1 - \frac{\text{Hemicellulose in pretreated solid residue}\ (\text{g})}{\text{Initial amount of hemicellulose in raw bamboo}\ (\text{g})}\right) \times 100 \quad \text{(S4)}$$

The concentrations of xylose in 100 μL of soluble liquid were diluted with ultrapure water and filtered through a 0.22 μm membrane before analysis using high-performance anion exchange chromatography (HPAEC, Dionex ICS 3000).

1.7.2 Fourier transform infrared spectroscopy (FT-IR) analysis

Fourier-transform infrared (FT-IR) spectra of pulp and acetylated products obtained from different pulping systems were recorded using an FT-IR spectrometer (Nicolet iN10 MX, Thermo Scientific). Approximately 1.0 wt% of each sample was thoroughly mixed with potassium bromide (KBr) and ground into a fine powder for pellet preparation. Spectra were collected over the range of 700–4000 cm^{-1} with a resolution of 4 cm^{-1}. The acetyl content (Ac%) was defined as the mass percentage of acetyl groups relative to the total mass of the acetylated cellulose. Ac% was calculated from the FT-IR spectra following the method reported by Brand et al.[4] Prior to calculation, all spectra were normalized, and each sample was scanned three times; the

average peak values were used for integration. The acetyl content was calculated using the following equation.[4]

$$A_c\ (\%) = \frac{H_{C=O}/H_{C-O}}{0.0282} \qquad \text{(S5)}$$

Here, $H_{C=O}$ represents the peak height of the acetyl group C=O around 1736 cm^{-1}, while H_{C-O} represents the peak height of the C-O around 1061 cm^{-1}.

1.6.3 Determination of Fock reactivity

A modified Fock method was employed to assess the reactivity of the dissolving pulp and to further evaluate differences among the samples, as described by Tian et al. [5] Briefly, 0.50 g of pre-moistened pulp was weighed, and wetted with a 9 wt% sodium hydroxide (NaOH) solution at 20 °C for 10 min. Subsequently, 1.3 mL of carbon disulfide (CS_2) was added, and the sulfonation reaction was carried out at 19 °C for 3 h to form a viscose solution. To reprecipitate the dissolved cellulose, 3 mL of 20 wt% sulfuric acid (H_2SO_4) was added with thorough mixing. The precipitate was then treated with 20 mL of 68 wt% H_2SO_4 and shaken for 1 h to ensure full acidification of the fibres. This was followed by the addition of a 0.17 mol/L potassium dichromate ($K_2Cr_2O_7$) solution to oxidize the precipitated cellulose. Afterwards, 5 mL of 10 wt% potassium iodide (KI) solution was added, and the liberated iodine was titrated with 0.10 mol/L sodium thiosulfate ($Na_2S_2O_3$). Once the solution turned yellowish brown, a starch indicator was added, and the titration continued until a sharp color change to blue-green indicated the endpoint. The Fock reactivity was defined as the mass percentage of dissolved cellulose in the pulp sample and was calculated using the following equation.[6]

$$\text{Dissolved cellulose}(\%) = \frac{\left\{v_1 \times c_1\left(v_2 \times c_2 \times \frac{100}{40}\right) \times \frac{1}{6}\right\} \times M \times \frac{1}{4} \times \frac{100}{10.4}}{m} \times 100 \qquad \text{(S6)}$$

M represents the molecular weight of the glucose unit (162 g/mol); m is the oven-dry mass of the pulp sample (g); v_1 is the volume of potassium dichromate ($K_2Cr_2O_7$) solution used (0.01 L); c_1 is the concentration of $K_2Cr_2O_7$ solution (0.17 mol/L); v_2 is

the volume of sodium thiosulfate ($Na_2S_2O_3$) solution consumed (L); and c_2 is its concentration (0.10 mol/L). The factor 100/40 accounts for the 40 mL aliquot taken from a 100 mL volumetric flask for titration. The term 1/6 reflects the stoichiometry, where six thiosulfate ions are consumed per dichromate ion reduced, and 1/4 accounts for four glucose units oxidized per dichromate ion. The term 100/10.4 accounts for the use of 10 mL (corresponding to 10.4 g) of the total 100 g sample solution in the final titration.

1.7.4 X-ray diffraction (XRD) analysis

The XRD patterns were recorded by using a multi-position automatic sampling X-ray diffractometer (D8 ADVANCE, Bruker, USA), and the data were measured in the range of 5° to 40° at a scanning rate of 2° min^{-1}. The relative crystallinity index (CrI) was calculated using Segal's method.[7]

$$\text{CrI}\ (\%) = \frac{\left(I_{200} - I_{\text{am}}\right)}{I_{200}} \times 100 \qquad \text{(S7)}$$

where I_{200} is the peak intensity of the (200) reflection, and I_{am} is the lowest intensity between the (110) and (200) peaks at approximately 18.7°.

1.7.5 Gel permeation chromatography (GPC) analysis

The absolute weight-average molecular weight (M_w) and molar-mass dispersity ($Đ_M$) of pulp and CA were determined by gel permeation chromatography (GPC) using a refractive index (RI) detector (Waters 2414) and a laser scattering (LS) detector (Wyatt DAWN HELEOS-II), following an established method.[8] The DI of the sample was obtained from the RI detector, while the M_w was obtained from the LS detector. Samples (15 mg) were first dissolved in 1 g of 1-butyl-3-methylimidazolium acetate (BmimAc)/dimethyl sulfoxide (DMSO) (1:1, w/w) at 25 °C for 1 h, followed by the addition of 9 g dimethylacetamide (DMAc) and further stirring for 0.5 h. The resulting 3 mg/mL solution was filtered (0.22 μm) before analysis. The mobile phase was BmimAc/DMSO/DMAc (1:1:18, w/w), and separation was performed using a PL-

Mixed C column with a Waters e2695 GPC system at a 1.0 mL/min flow rate. All measurements were conducted in triplicate.

1.7.6 Accessibility of pulping

A modified Direct Red 28 dye adsorption method was used to assess the fiber accessibility of pulps derived from different pulping systems. Specifically, 0.1 g of each pulp sample was incubated with 10 mL of DR 28 solutions at various concentrations (0, 0.05, 0.1, 0.5, 1.0, 2.0, 3.0, and 4.0 g/L) at 50 °C and 150 rpm for 24 h. After incubation, the supernatant was collected, and the residual dye concentration was determined by UV–vis spectroscopy at 498 nm. The amount of dye adsorbed was calculated using a standard calibration curve. The Langmuir adsorption isotherm was applied to model the adsorption behavior and evaluate the fiber accessibility of the pulps. Construction of the standard curve is shown in **Fig. S3**†.

1.7.7 Morphological analysis

The morphology of the screened pulp was observed using a scanning electron microscope (Regulus8100, Hitachi, Japan) with 3.0 kV of acceleration voltage.

1.7.8 Diffusion-edited ^{1}H NMR spectroscopy

The diffusion-edited ^{1}H NMR spectra of the various CA samples were acquired following the previous literature. Approximately 20 mg of each sample was dissolved in 1.0 g of deuterated dimethyl sulfoxide (DMSO-d_6) mixture at 65 °C until complete dissolution. The prepared solutions were then subjected to diffusion-edited ^{1}H NMR analysis.

1.7.9 Hazen test

Various CA samples (B/F-CA, KP-CA, C-CA) were dissolved in dichloromethane/methanol solutions to prepare 3% (w/v) solutions. The color parameters (L, a, b) and hazen values were measured using a spectrophotometer (HACH/LICO 620) in accordance with ISO 7027-198. Each sample was tested in triplicate, and the average values were reported.

1.7.10 2D-HSQC NMR spectroscopy.

In detail, approximately 30 mg of lignin was dissolved in 0.5 mL of DMSO-d_6. Then the sample was tested using an NMR spectrometer (AVANCE NEO 400M, Bruker, Germany) for 4 h.

1.7.11 ^{31}P NMR spectroscopy.

Quantitative ^{31}P NMR spectroscopy was performed following the established protocol.[9] Briefly, 20 mg of lignin was dissolved in 500 μL of a solvent mixture consisting of anhydrous pyridine and deuterated chloroform (1.6:1, v/v) under stirring. Subsequently, 100 μL of cyclohexanol solution (10.85 mg/mL in the same solvent mixture) was added as the internal standard, along with 100 μL of chromium (III) acetylacetonate solution (5 mg/mL) as the relaxation agent. The mixture was then reacted with 100 μL of the phosphitylating reagent 2-chloro-4,4,5,5-tetramethyl-1,3,2-dioxaphospholane (TMDP) for approximately 10 min. The resulting solution was transferred to a 5 mm NMR tube for ^{31}P NMR analysis.

1.7.12 GPC analysis of lignin.

The weight-average (M_w) and number-average (M_n) molecular weights and molar-mass dispersity ($Đ_M$=M_w/M_n) of the lignin samples were determined by gel permeation chromatography (GPC) using an Agilent 1200 system (Agilent Technologies, USA) equipped with a UV detector operating at 240 nm. Separation was performed on a PL-gel 10 μm Mixed-B column (7.5 mm i.d.), and molecular weights were calculated based on calibration with polystyrene standards, following established protocols.[10]

1.7.13. Other analyses

The morphologies of LCNFs and LNPs were examined using high-resolution transmission electron microscopy (HRTEM, JEM-F200, JEOL, Japan), and particle size was analyzed with ImageJ software (National Institutes of Health).

The Barrett-Joyner-Halenda (BJH) pore volumes and Brunauer-Emmett-Teller (BET) areas of pretreated residues were measured using a surface area analyzer (Kubo-X1000, Builder Electronic Technology Co., Ltd., China).

The zeta potential and polydispersity of lignin and emulsion were measured using a Malvern Zetasizer Nano ZS (Malvern Instruments, UK), with three replicates per sample.

According to the Chinese National Standard GB/T 33333-2016, tensile tests on the overlapped wooden specimens were conducted using a universal testing machine (UTM6530, Shenzhen Sanyang Technology Co., Ltd.). The water resistance of wood adhesives was evaluated by tensile testing of overlapped specimens at 25 °C after 24 h immersion in water. Extreme resistance was assessed by tensile testing after exposure at −45 °C and 180 °C for 2 h. Aging resistance was determined by tensile testing after storage at 90 °C and 50% relative humidity for one week.

The FA content in the concentrate was determined by acid-alkali titration. A 0.3 g portion of the concentrate was diluted 200-fold with distilled water, and approximately 2 mL of phenolphthalein solution (10 g/L) was added as an indicator. The FA content was then determined by titration with 1 mol/L NaOH. The BTEAC content was measured by precipitation titration. Specifically, 0.2 g of concentrate was diluted 200-fold with distilled water, and the resulting solid precipitate was filtered to avoid interference with the titration endpoint. After neutralization with 1 mol/L NaOH, about 3 mL of 2% starch solution and 2 mL of 0.5% fluorescent yellow indicator were added successively, followed by titration with 0.1 mol/L $AgNO_3$ to precipitate Cl^- from BTEAC. The recovered DES was reused in the next cycle after replenishing the lost components based on the remaining mass after separation.

$$\text{FA recovery yield (\%)} = \frac{\text{Mass of recycled FA}}{\text{Total mass of FA}} \times 100 \quad \text{(S8)}$$

$$BTEAC \text{ recovery yield } (\%) = \frac{\text{Mass of recycled } BTEAC}{\text{Total mass of BTEAC}} \times 100 \quad \text{(S9)}$$

1.8 Mass balance

$$\text{Cellulose acetate yield } (\%) = \frac{\text{Actual mass obtained after acetylation}}{\text{Mass of bleached bamboo pulp}} \times 100 \quad \text{(S10)}$$

$$\text{LNPs yield } (\%) = \frac{\text{Mass of LNPs remaining after freeze - drying}}{\text{Mass of DES lignin added in the preparation of LNPs}} \times 100$$

11)

The average value of bamboo dissolving pulp obtained after bleaching 1g of cellulose-rich residue was 0.8767±0.1274 g.

Bleached bamboo dissolving pulp yield = (0.8767 g/1g) *100%=87.67%

The average value of cellulose acetate solids prepared by acetylation with 1g of bleached bamboo pulp was 1.3042 ± 0.0813 g.

Cellulose acetate yield = (1.3042 g/1 g) *100%=130.42%

41.01 kg of cellulose-rich residue to obtain cellulose acetate yield=41.01 kg*87.67%*130.4%=46.88 kg

30 mg of lignin with a removal rate of 90.7% was recovered to obtain 25.596 mg

Recovery DES lignin yield = (25.5960 mg/30 mg) *100%=85.32%

The solution of LNPs containing 30 mg of DES lignin was freeze-dried to obtain a solid with an average of 29.6009 ± 0.1355 mg.

LNPs yield = (29.6009 mg/30mg) *100%=98.67%

21.76 kg DES lignin LNPs yield=21.76 kg *85.32%*98.67%=18.32 kg

1.9 Calculation of energy consumption in the DES cooking process

A 10 L digester typically produced approximately 1 kg of DES pulp. The energy consumption of the DES pulping process was estimated based on a method proposed by Wang et al., which established a linear relationship between heating power and temperature.[11] At a maximum heating power of 600 W, the hotplate reached 340 °C,

corresponding to an estimated power requirement of 229.4 W to maintain 130 °C. Thus, the total energy consumption for 2 h cooking period was calculated as 229.4 W×2.0 h=0.458 kWh. For comparison, the energy consumption of the sulfate pulping process under similar conditions (160 °C, 2 h) was estimated to be 0.620 kWh. Based on data from the World Nuclear Association, the associated CO_2 emissions were 0.375 kg CO_2/kg of pulp for DES pulping and 0.508 kg CO_2/kg of pulp for sulfate pulping. Therefore, DES pulping resulted in approximately 26.18% lower CO_2 emissions compared to the conventional sulfate process, highlighting its potential advantages in terms of environmental sustainability.[12]

1.10 Economic calculation

To assess the economic feasibility of producing cellulose acetate–grade dissolving pulp with BTEAC/FA, we performed economic calculations for the entire process and compared the results with a rough cost estimate based on the process of Chen et al. and with an industrial method currently used for cellulose acetate–grade pulp production. The overall cost primarily comprises the feedstocks, chemical cost, energy cost, and water cost [13]. The energy cost is calculated as the product of the electricity consumption for treating 1 ton of dissolving pulp and the electricity price [14]. The electricity consumption (EC) is calculated by the following formula:

$$EC = P_{max} \times T \quad (1)$$

Where P_{max} represents the maximum power of the equipment, Kw. T is the total time spent on treating 1 ton of dissolving pulp, h. Thus, the energy cost (E) is determined by the following formula:

$$E = EC \times EP \quad (2)$$

Where EC is the electricity consumption for treating 1 ton of dissolving pulp, Kw·h. EP is the electricity price, 0.06, \$/Kw·h.[13]

2. Tables

Table S1. Lignin recovery rate of ChCl/LA system under different treatment conditions.

Table S2. Lignin recovery rate of BTEAC/FA system under different treatment conditions.

Table S3. Lignin recovery rate of PTSA/H_2O system under different treatment conditions.

Table S4. Lignin recovery rate of GVL/H_2O system under different treatment conditions.

Table S5. Chemical composition of the original and after cooking using different pulping systems.

Table S6. A comprehensive comparison of pulp quality obtained by the BTEAC/FA pulping method, conventional pulping methods, and other novel pulping systems.

Table S7. Chemical composition of pulp obtained from different pulping systems after bleaching.

Table S8. Conversion of acetyl content to the degree of substitution calculated from the intensity of specific peak positions in the FTIR spectra.

Table S9. Relative integration results of diffusion-edited ^{1}H NMR spectra.

Table S10. L, a, b values and hazen of various types of C in dichloromethane/methanol solution.

Table S11. Degree of substitution and esterification of cellulose acetate produced by different pulp or cellulose extraction methods.

Table S12. Purity of lignin under optimal cooking conditions of different pulping systems.

Table S13. Molecular weight of lignin under optimal cooking conditions of different pulping systems.

Table S14. Quantification of the different hydroxyl groups in lignin fractions by quantitative ^{31}P NMR spectroscopy (mmol/g lignin).

Table S15. Zeta potential and polydispersity of the corresponding Pickering emulsions at different R-L lignin additions (0.075, 0.100, and 0.125 wt%) on different storage times.

Table S16. pH and viscosity of recycled DES waste liquid.

Table S17. Approximate contents of BTEAC, FA, and H_2O of recycled DES waste liquid.

Table S18. The characteristics of unbleached and bleached pulp obtained by BTEAC/FA-based DES after four cycles.

Table S19. Zeta potential and polydispersity of the corresponding Pickering emulsions stabilized by lignin nanoparticles prepared after four DES pulping cycles at R-L lignin additions (0.1 wt%).

Table S20. Mechanical properties of prepared adhesives for wood bonding after immersion in water at 25°C for 24 h.

Table S21. Mechanical properties of prepared adhesives for wood bonding after aging at 90°C and 50% humidity for one week.

Table S22. Estimated production costs for producing 1 ton of cellulose acetate-grade dissolving pulp using our optimal process.

Table S23. Estimated cost of producing 1 ton of cellulose acetate-grade dissolving pulp using Chen et al.'s optimal process.[15]

Table S24. Estimated cost of producing one ton of cellulose acetate-grade dissolving pulp using the current industrial process.

3. Figures

Schematic diagram S1. Biomass-derived or synthetic pathways of hydrogen bond donors and acceptors in DESs [41-48]. (a) Choline chloride. (b) Formic acid. (c) Oxalic acid (d) Lactic acid.

Fig. S1. Digital images of cooking reagents used in different pulping systems. (a) Freshly prepared cooking reagent. (b) The same reagent after standing for 24 h.

Fig. S2. Schematic flow of the pulping process and subsequent utilization of by-products. (a) Cellulose is separated and bleached to obtain high-purity dissolving pulp for cellulose acetate production. Lignin is recovered and processed into nanoparticles for stabilizing Pickering emulsions, while hemicellulose is hydrolyzed into xylose, and DES was recycled for four cycles and finally used as a wood adhesive. (b) Proposed processes and mechanism of LNPs formation and emulsion stabilization.

Fig. S3. Calibration plot of dye concentration associated with UV absorbance.

Fig. S4. Chemical composition of pulps produced by different cooking systems. (a) ChCl/LA system. (b) BTEAC/FA system. (c) *p*-TsOH/water system. (d) GVL/water system.

Fig. S5. Morphology of pulp obtained under the optimal pulping conditions of different pulping systems. (a) Visual image. (b) SEM images.

Fig. S6. (a) TGA curves and (b) DTG curves of pulps obtained from different pulping systems.

Fig. S7. Side-chain region and aromatic region in the 2D-HSQC NMR of the lignin obtained under optimal cooking conditions of different pulping systems.

Fig. S8. Quantitative ^{31}P NMR spectra of DEL and lignin obtained under optimal cooking conditions of different pulping systems.

Fig. S9. FT-IR spectrum of lignin obtained under optimal cooking conditions of different pulping systems.

Fig. S10. TEM images of LNPs at different magnifications prepared by acetone rotary evaporation.

Fig. S11. Photographs of LNPs and its Tyndall were from kraft lignin (L-KP-160-2) and DES lignin (L-B/F-130-2). (a) Image of L-KP-160-2. (b) Image of (a) after 24 h of standing. (c) Tyndall effect of L-KP-160-2. (d) Image of L-B/F-130-2. (e) Image of (d) after 24 h of standing. (f) Tyndall effect of L-B/F-130-2.

Fig. S12. (a) Emulsions prepared with different oil-water ratios (from left to right oil/water ratios are 7:3, 6:4, 5:5, 4:6, 3:7). (b) Microscopic image of the corresponding emulsions.

Fig. S13. Lignin nanoparticles are used to stabilize Pickering emulsions. (a) Visual image on day 5. (b) Microscopic image on day 5. (c) Particle-size distribution on day 5. (d) Visual image after 35 days of storage. (e) Microscopic image after 35 days of storage.

Fig. S14. Content of aqueous phase inhibitors and degradation products in DES waste liquor.

Fig. S15. Comparison of the crystal structure and crystallinity of bleached and unbleached pulps obtained after four DES cycles compared to the initial pulp.

Fig. S16. Pickering emulsions stabilized by lignin nanoparticles prepared after four DES pulping cycles at R-L lignin additions (0.1 wt%). (a) Visual image on day 1. (b) Microscopic image on day 1. (c) Particle-size distribution on day 1. (d) Visual image after 15 days of storage. (e) Microscopic image after 15 days of storage. (f) Particle-size distribution after 15 days of storage.

Fig. S17. Stress-strain curves of the prepared adhesive for wood bonding.

Fig. S18. Mechanical properties of prepared adhesives for wood bonding under extreme conditions.

Table S1. Lignin recovery rate of ChCl/LA system under different treatment conditions.

Samples	Lignin recovery ratio (%)
C/L-100-2	76.33±1.55
C/L-110-2	72.69±1.23
C/L-120-2	74.23±1.15
C/L-130-2	71.55±0.85
C/L-140-2	63.45±0.72

Table S2. Lignin recovery rate of BTEAC/FA system under different treatment conditions.

Samples	Lignin recovery ratio (%)
B/F-100-2	81.83±1.21
B/F-110-2	76.16±1.89
B/F-120-2	76.58±1.56
B/F-130-2	85.32±1.38
B/F-140-2	95.31±0.93

Table S3. Lignin recovery rate of *p*-TsOH/H_2O system under different treatment conditions.

Samples	Lignin recovery ratio (%)
P-60-1	82.02±1.29
P-70-1	88.18±1.56
P-80-1	85.30±0.85
P-90-1	87.20±2.06
P-100-1	70.60±1.33

Table S4. Lignin recovery rate of GVL/H_2O system under different treatment conditions.

Samples	Lignin recovery ratio (%)
G-180-2	69.65±1.26
G-200-2	83.50±1.43
G-220-2	88.13±0.58
G-230-2	87.51±2.41
G-240-2	94.49±0.32

Table S5. Chemical composition of the original and after cooking using different pulping systems.

Samples	Cellulose (%)	Hemicelluloses (%)	Lignin (%)	Pulp yield (%)	Degree of polymerization (DP)
Raw	44.64±0.78	14.76±0.73	23.99±0.49	/	/
C/L-130-2	78.47±0.92	6.58±1.23	7.35±0.44	54.47±0.93	986±2
B/F-130-2	84.74±1.01	1.35±0.64	4.61±0.57	48.40±0.86	1024±4
P-90-1	90.23±1.84	1.63±1.84	4.71±0.86	47.27±0.59	1029±4
G-220-2	85.39±0.98	1.36±0.12	4.87±0.46	38.35±0.25	758±3
KP-160-2	75.55±1.19	11.82±0.43	4.83±0.28	53.47±0.55	1270±5

/ indicates that no detection.

Table S6. A comprehensive comparison of pulp quality obtained by the BTEAC/FA pulping method, conventional pulping methods, and other novel pulping systems.

Raw material	Pulping method (%)	Pulping conditions	Pulp or residue yield (%)	Cellulose content (%)	Hemicellulose content (%)	Ref
Poplar	FA-phenol-water	120 ℃, 2 h	/	98.95	0	[16]
Eucalyptus slabs	BTEAC/FA	130 ℃, 2 h	53.83	<90.00	>2.00	[17]
Eucalyptus	ChCl/LA,20 vol%	140 ℃, 4 h	60.11	<80.00	>5.00	[18]
Sugarcane bagasse	ChCl:PTSA:EG	90 ℃, 35 min	20.00	97.07	0	[19]
Bamboo shoot shells	BTEAC/FA	120 ℃,20 min	48.1	72.5	4.8	[20]
Spruce	ChCl/LA	130℃,4.5 h	45.82	/	/	[21]
Moso bamboo	*P*-TsOH	90 ℃, 1h	<40.00	82.36	7.4	[22]
Birch wood chips	75 wt% GVL	140 ℃, 210 min	53.4	68.9	24.7	[23]
Scots pine	ChCI-LA-Gly	155 ℃, 4 h	40.0	70.6	13.9	[24]
Poplar wood chips	ChCI/LA	140 ℃, 1 h	<60.00	<70.00	>10.00	[25]
Eucalyptus	PA:U/25 wt% PTSA	90 ℃, 8 h	59.50	/	/	[26]
Rice straw	K_2CO_3-Gly	140 ℃, 100 min	/	73.8	19.9	[27]
Bamboo	NaOH＋Na_2S	160 ℃, 2h	53.47	75.55	11.82	Control sample
Bamboo	BTEAC/FA	130 ℃, 2h	48.40	84.74	1.35	This work

/ indicates that no detection.

Table S7. Chemical composition of pulp obtained from different pulping systems after bleaching.

Samples	Cellulose (%)	Hemicelluloses (%)	Lignin (%)	DP
Raw	44.64±0.78	14.76±0.73	23.99±0.49	/
C/L-130-2-BP	87.58±1.56	6.12±0.37	/	741±6
B/F-130-2-BP	97.36±2.15	0.14±0.03	/	583±3
P-90-1-BP	94.91±1.84	0.15±0.05	/	637±2
G-220-2-BP	80.04±2.56	0.13±0.03	/	440±1
KP-160-2-BP	86.28±2.01	10.19±0.38	/	670±5

/ indicates that no detection.

Table S8. Conversion of acetyl content to degree of substitution calculated from the intensity of specific peak positions in the FTIR spectra.

Samples	Relative integration results (degree of substitution)
B/F-CA	2.92±0.04
KP-CA	2.82±0.09
C-CA	2.89±0.07

Samples	Relative integration results (degree of substitution)
B/F-CA	2.86±0.03
KP-CA	2.82±0.04
C-CA	2.93±0.09

Table S9. Relative integration results of diffusion-edited ^{1}H NMR spectra.

Table S10. L, a, b values and hazen of various types of C in dichloromethane/methanol solution.

Samples	L	a	b	Hazen
C-CA	95.4±0.20	-1.5±0.01	8.6±0.05	248.0±1.00
KP-CA	92.3±0.15	-1.4±0.05	10.2±0.10	310.5±2.50
B/F-CA	98.9±0.10	0.0±0.01	0.7±0.01	21.5±0.50

Table S11. Degree of substitution and esterification of cellulose acetate produced by different pulp or cellulose extraction methods.

Methods of obtaining pulp or cellulose	Type of cellulose acetate	Degree of substitution (DS)	Esterification degree (%)	Ref
ZAC-EG-treated cotton pulp	DAC	2.4	39.4	[28]
$ZnCl_2$-LA treated bamboo BKP	TAC	2.84	42.4	[29]
ChCl-OA treated bamboo BKP	TAC	2.87	42.7	[30]
Soda-AQ and D_1EP treated paper mulberry	DAC	2.66	40.8	[31]
H_2O_2-Alkaline treated Banknotes	DAC	2.38		[32]
Sugarcane straw treated Acids and alkalis	DAC	2.72	-	[33]
H_2O_2-Alkaline	TAC	2.91	-	[34]
$NaClO_2$-Acidic	TAC	2.9	45.0	[35]
H_2O_2-Alkaline	DAC	2.6	41.0	[36]
H_2O_2-Alkaline	DAC and TAC	2.08–2.82	-	[37]
NaOH+Na_2S	TAC	2.67	40.0	[38]
BTEAC/FA-DES	TAC	2.92	-	This work

Abbreviations: DAC: cellulose diacetate, DS: degree of substitution, ED: esterification degree; TAC: cellulose triacetate.

Table S12. Purity of lignin under optimal cooking conditions of different pulping systems.

Samples	Lignin		Cellulose	Hemicelluloses
	Klason lignin	Acid-soluble lignin		
L-C/L-130-2	85.91±0.52	0.74±0.04	3.66±0.43	0.31±0.18
L-B/F-130-2	90.76±0.46	1.33±0.03	3.36±0.57	0.35±0.14
L-P-90-1	76.31±0.75	0.70±0.01	3.57±0.31	0.40±0.25
L-G-220-2	91.02±0.23	1.60±0.03	3.73±0.22	0.35±0.14
L-KP-160-2	73.90±0.81	1.62±0.02	6.18±0.86	7.10±0.56

Purity analysis showed that L-B/F-130-2 and L-G-220-2 had high lignin purity (>92%) with minimal hemicelluloses contamination, while L-KP-160-2 contained only 75.5% lignin, along with 6.18% cellulose and 7.10% hemicelluloses, indicating lower selectivity of the kraft process **(Table S11†)**.

Table S13. Molecular weight of lignin under optimal cooking conditions of different pulping systems.

Samples	M_w (g/mol)	M_n (g/mol)	$Đ_M$ (M_w/ M_n)
DEL	7450±56	4257±22	1.75
L-C/L-130-2	2356±18	1293±8	1.82
L-B/F-130-2	2302±23	1370±12	1.68
L-P-90-1	4490±19	2041±20	2.20
L-G-220-2	1621±5	870±9	1.86
L-KP-160-2	1964±10	1278±8	1.54

The molecular weight and distribution of lignin byproducts are important evaluation criteria for measuring their application potential. As shown in **Fig. 6b and Table S12†**, the M_w of DEL was 7450 g/mol, significantly higher than those of all regenerated lignin fractions. This difference is attributed to partial cleavage of ester linkages in LCCs during the cooking process, resulting in the depolymerization of lignin macromolecules. Among the samples, L-G-220-2 and L-KP-160-2 exhibited relatively low M_w of 1621 and 1964 g/mol respectively, indicating that high cooking temperatures facilitated extensive lignin depolymerization into low-molecular-weight fragments. The M_w of L-C/L-130-2 and L-B/F-130-2 are in the middle, indicating that mild conditions are conducive to the retention of lignin molecular chains, while the high M_w of L-P-90-1 may be attributed to the condensation of lignin caused by strong acidic conditions, which is consistent with the disappearance of the S-type structural unit of the lignin signal in the 2D-HSQC spectrum. In addition, the $Đ_M$ of L-B/F-130-2 is 1.68, which is the lowest among the emerging pulping systems in this study, indicating that it has a uniform molecular weight distribution. The narrow molecular

weight distribution can be an ideal feedstock for further conversion to high-value products such as poly urethanes and carbon fibers.[39, 40]

Table S14. Quantification of the different hydroxyl groups in lignin fractions by quantitative ^{31}P NMR spectroscopy (mmol/g lignin).

Samples	Aliphatic OH	Syringyl OH		Guaiacyl OH		*p*-hydroxyphenyl OH	Carboxylic Group	Total phenolic OH
		C [a]	NC [b]	C [a]	NC [b]			
DEL	4.06	0.17	0.26	0.09	0.37	0.73	0.19	1.61
L-C/L-130-2	2.03	0.32	0.74	0.19	0.53	0.88	0.34	2.66
L-B/F-130-2	0.94	0.44	0.97	0.31	0.67	0.88	0.29	3.28
L-P-90-1	0.91	0.49	0.71	0.31	0.59	0.60	0.45	2.71
L-G-220-2	1.47	0.38	0.99	0.29	0.90	0.76	0.28	3.32
L-KP-160-2	2.64	0.30	1.07	0.33	0.75	0.37	0.63	2.82

[a] C=Condensed 5-substitued lignin.

[b] NC = Non-condensed.

[c] Total phenolic hydroxyl group =Syringyl OH, Guaiacyl OH and p-hydroxyphenyl OH.

Table S15. Zeta potential and polydispersity of the corresponding Pickering emulsions at different R-L lignin additions (0.075, 0.100, and 0.125 wt%) on different storage times.

Dosage of Lignin (wt%)	Zeta potential（mV）		Polydispersity (PDI)		
	Day 1	Day 15	Day 1	Day 15	Day 35
0.075	-12.3±0.58	-10.5±0.51	0.391±0.084	0.502±0.132	0.813±0.157
0.100	-19.8±0.59	-22.1±0.34	0.269±0.092	0.351±0.077	0.525±0.538
0.125	−24.2±0.22	−27.6±0.47	0.243±0.056	0.321±0.071	0.449±0.120

Table S16. pH and viscosity of recycled DES waste liquid.

Samples	Viscosity (mPa·s)	pH
BTEAC/FA	10.2	2.17 (Diluted 30 times)
R0-WL	7.2	2.21
R1-WL	48.0	2.32
R2-WL	84.6	2.43
R3-WL	145.2	2.46
R4-WL	201.6	3.27

Table S17. Approximate contents of BTEAC, FA, and H_2O of recycled DES waste liquid.

Samples	BTEAC (%)	FA (%)	H_2O (as % of initial reagent mass)
R0-WL	95.2	83.7	2.6
R1-WL	92.8	74.6	3.5
R2-WL	91.7	65.4	4.8
R3-WL	89.6	51.0	7.6
R4-WL	89.8	38.2	10.3

Table S18. The characteristics of unbleached and bleached pulp obtained by BTEAC/FA-based DES after four cycles.

Samples	DP	α-cellulose (%)	Alkali-soluble substances (%)	Brightness (%)
R4-P	1115	81.26	6.38	/
R4-BP	629	85.11	4.54	78.7

/ indicates that no detection.

Table S19. Zeta potential and polydispersity of the corresponding Pickering emulsions stabilized by lignin nanoparticles prepared after four DES pulping cycles at R-L lignin additions (0.1 wt%).

Samples	Zeta potential（mV）			Polydispersity (PDI)		
	Day 1	Day 15	Day 105	Day 1	Day 5	Day 105
R4-L	−23.56±0.42	−24.97±0.65	−26.44±0.78	0.212±0.046	0.224±0.079	0.329±0.033

Table S20. Mechanical properties of prepared adhesives for wood bonding after immersion in water at 25°C for 24 h.

/ indicates not detected

Samples	Tensile strength (MPa)
PVA	/
R4-WL	/
R4-WL/PVA	1.60±0.74

Table S21. Mechanical properties of prepared adhesives for wood bonding after aging at 90°C and 50% humidity for one week.

Samples	Tensile strength (MPa)
PVA	1.96±0.88
R4-WL	/
R4-WL/PVA	6.26±1.34

/ indicates not detected

Table S22. Estimated production costs for producing 1 ton of cellulose acetate-grade dissolving pulp using our optimal process.

Feedstocks	Price ($/t)	Consumption (t)	Cost ($)	Source
Neosinocalamus affinis (Oven-dry)	63~90	2.4	151~216	https://detail.1688.com/offer/1190074200.html?_t=1758889166389&spm=a2615.7691456.co_0_0_wangpu_score_0_0_0_0_1_0_0000_0.0
BTEAC	2100	13.0	27300	https://www.100ppi.com/mprice/plist-1-6031-1.html
Formic acid	322	10.5	3381	https://www.100ppi.com/mprice/company-1726-308694-1.html
Sodium hypochlorite (10% sol.)	70	0.57	40	https://www.100ppi.com/news/detail-20250919-4783102.html
H_2O_2	168~207	0.25	42~52	https://product.11467.com/info/2552554.htm
NaOH	322~420	0.01	3~4	https://www.chemicalbook.com/priceinfoall_cb8105015.htm
Water	0.59	63.9	38	https://www.beijing.gov.cn/fwcj/jiage/ggfw1/661ccdcc81e5641581784c4f.html
Electricity	0.06/kWh	600.0	36	https://fgw.beijing.gov.cn/bmcx/djcx/jzldj/202110/t20211025_2520169.htm
Total cost	$ (30991~31067) /t			

Table S23. Estimated cost of producing 1 ton of cellulose acetate-grade dissolving pulp using Chen et al.'s optimal process.[15]

Feedstocks	Price ($/t)	Consumption (t)	Cost ($)	Source
Eucalyptus chips (Oven-dry)	40~110	2.7	108~297	https://www.alibaba.com/product-detail/Eucalyptus-Wood-Chips-Eucalyptus-Wood-Chips_10000024329244.html?spm=a2700.galleryofferlist.normal_offer.d_title.6a6413a0WfQVtH&priceId=c8ab086ce728449f8b7c34a2d2132970
Lactic acid	1120	24.8	27776	https://m.guidechem.com/product/prodetail27719902.html
Choline chloride	1681~2101	2.3	3866~4832	https://www.chemicalbook.com/SupplyInfo_1867353.htm
NaOH	322~420	0.57	184~239	https://www.chemicalbook.com/priceinfoall_cb8105015.htm
Na_2S	364~434	0.12	44~52	https://www.100ppi.com/news/detail-20250919-4782938.html
ClO_2	3711	0.009	33	https://chem.100ppi.com/price/plist-3866-1.html
H_2O_2	168~207	0.003	0.50~0.62	https://product.11467.com/info/2552554.htm
Water	0.59	150.0	89	https://www.beijing.gov.cn/fwcj/jiage/ggfw1/661ccdcc81e5641581784c4f.html
Electricity	0.06/kWh	4500	270	https://fgw.beijing.gov.cn/bmcx/djcx/jzldj/202110/t20211025_2520169.htm
Total cost	$ (32371~33589) /t			

Table S24. Estimated cost of producing one ton of cellulose acetate-grade dissolving pulp using the current industrial process.

Feedstocks	Price ($/t)	Consumption (t)	Cost ($)	Source
Neosinocalamus affinis (Oven-dry)	63~90	3.0~3.4	207~306	https://detail.1688.com/offer/1190074200.html?_t=1758889166389&spm=a2615.7691456.co_0_0_wangpu_score_0_0_0_0_1_0_0000_0.0
NaOH	322~420	0.20~0.29	64~122	https://www.chemicalbook.com/priceinfoall_cb8105015.htm
Na_2S	364~434	0.05~0.06	18~26	https://www.100ppi.com/news/detail-20250919-4782938.html
ClO_2	3711	0.03~0.05	111~186	https://chem.100ppi.com/price/plist-3866-1.html
H_2O_2	168~207	0.01~0.02	2~4	https://product.11467.com/info/2552554.htm
O_2	130	0.02~0.04	3~5	http://www.eairmall.com/
Steam	31~41	10~12	310~492	http://www.szwz.gov.cn/szwz/jggs/202509/af5faedfad7441228b338ed5a4c62d00.shtml
Water	0.59	30~50	18~30	https://www.beijing.gov.cn/fwcj/jiage/ggfw1/661ccdcc81e5641581784c4f.html
Electricity	0.06/kWh	900~1200	54~72	https://fgw.beijing.gov.cn/bmcx/djcx/jzldj/202110/t20211025_2520169.htm
Wastewater treatment	0.35	50~80	18~28	https://m.gepresearch.com/80/view-823950-1.html
Total cost	$ (805~1271) /t			

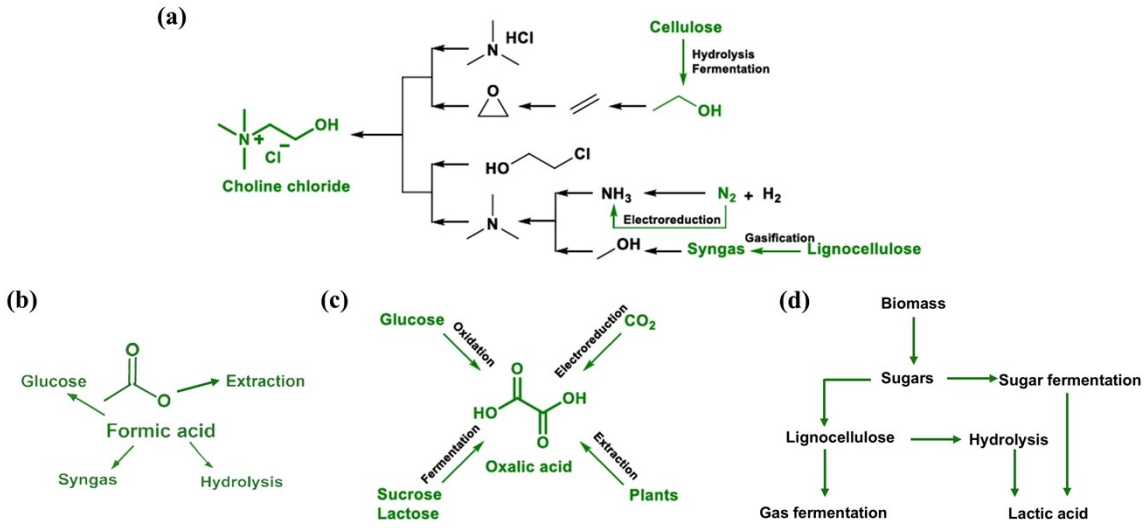

Schematic diagram S1. Biomass-derived or synthetic pathways of hydrogen bond donors and acceptors in DESs [41-48]. (a) Choline chloride. (b) Formic acid. (c) Oxalic acid (d) Lactic acid.

Most components involved in the DES systems used in this study, including choline chloride, formic acid, and lactic acid, are either directly obtained from biomass or produced through mature biomass-based processes. As illustrated in Schematic Diagram S1, formic acid (FA) can be generated from renewable feedstocks via catalytic oxidation of carbohydrates or hydrolysis of sugars and lignocellulosic materials.[49-53] These routes are well established in biomass valorization research and have been demonstrated to be efficient and scalable.[54-56] Choline chloride and lactic acid used in the ChCl/LA DES system can also be synthesized by biological fermentation or through catalytic upgrading of biomass-derived intermediates. Although benzyltriethylammonium chloride (BTEAC) is currently synthesized mainly from petrochemical feedstocks, such as by quaternization of triethylamine with benzyl chloride (CN103896781A), no bio-based synthetic pathways have yet been reported. However, progress in the development of bio-derived amines and renewable alkylation chemistry suggests that the future establishment of sustainable routes for quaternary ammonium salts is feasible. In addition, the low molar proportion of BTEAC in the

DES formulation (1:4) ensures that the majority of the solvent matrix remains composed of biomass-derived components.

In addition, the DES components used in this work exhibit low volatility. Although pure formic acid possesses a moderate vapor pressure, its incorporation as a hydrogen-bond donor within the DES results in the formation of an extensive hydrogen-bond network that stabilizes the liquid phase. This network substantially suppresses formic acid evaporation and reduces the saturated vapor pressure of the system. The immobilization of this volatile component minimizes inhalation risk and operational hazards and also decreases potential emissions during use.

Moreover, although BTEAC itself is not derived from biomass, its structural characteristics provide functional advantages for lignin solubilization. The benzyltriethylammonium cation interacts strongly with lignin through π–π interactions between its benzyl ring and lignin aromatic units, together with electrostatic interactions between the quaternary ammonium headgroup and polar or charged lignin fragments. These interactions disrupt π–π stacking, hydrophobic associations, and hydrogen-bonding networks within lignin and thereby facilitate fragmentation and dissolution of lignin fractions. This mechanistic behavior accounts for the strong lignin-removal capability of BTEAC-containing acidic DESs while preserving cellulose integrity.

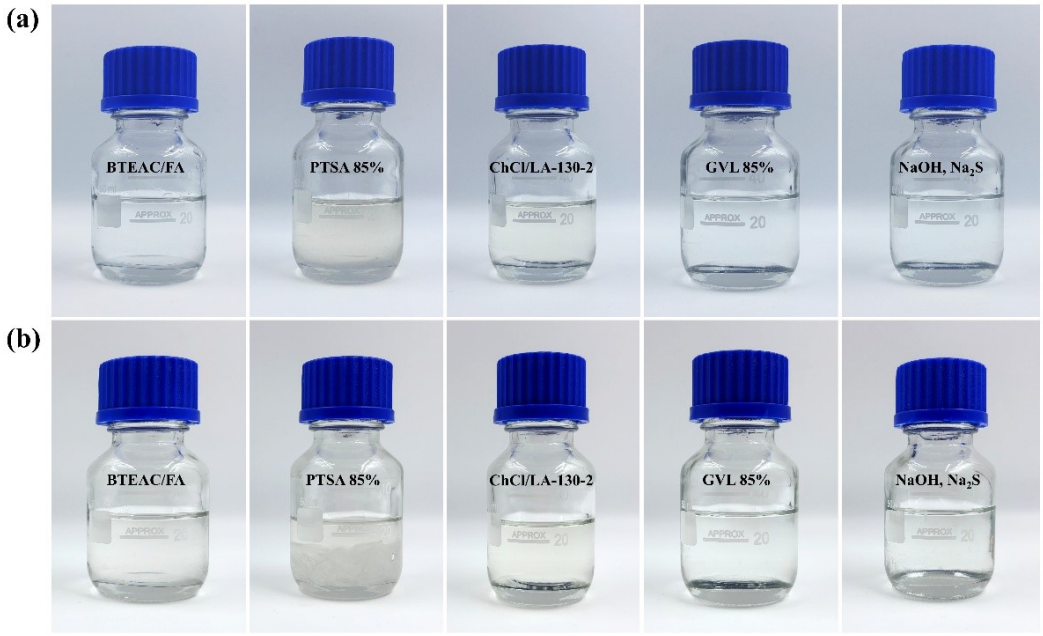

Fig. S1. Digital images of cooking reagents used in different pulping systems. (a) Freshly prepared cooking reagent. (b) The same reagent after standing for 24 h.

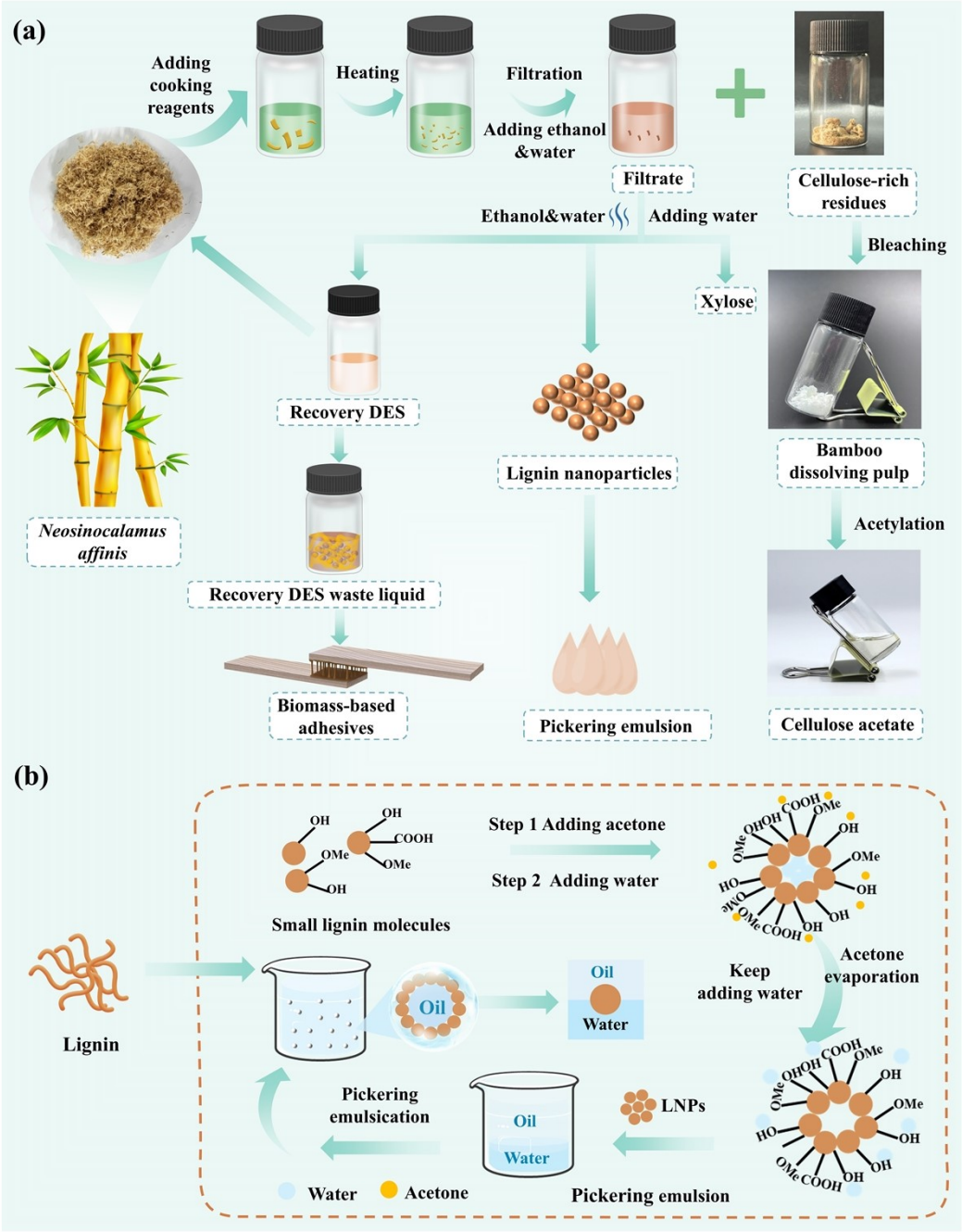

Fig. S2. Schematic flow of the pulping process and subsequent utilization of by-products. (a) Cellulose is separated and bleached to obtain high-purity dissolving pulp for cellulose acetate production. Lignin is recovered and processed into nanoparticles for stabilizing Pickering emulsions, while hemicellulose is hydrolyzed into xylose, and

DES was recycled for four cycles and finally used as a wood adhesive. (b) Proposed processes and mechanism of LNPs formation and emulsion stabilization.

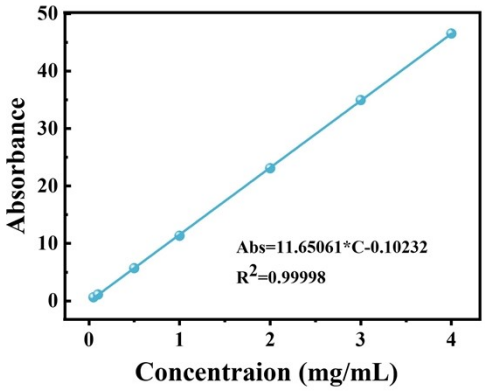

Fig. S3. Calibration plot of dye concentration associated with UV absorbance.

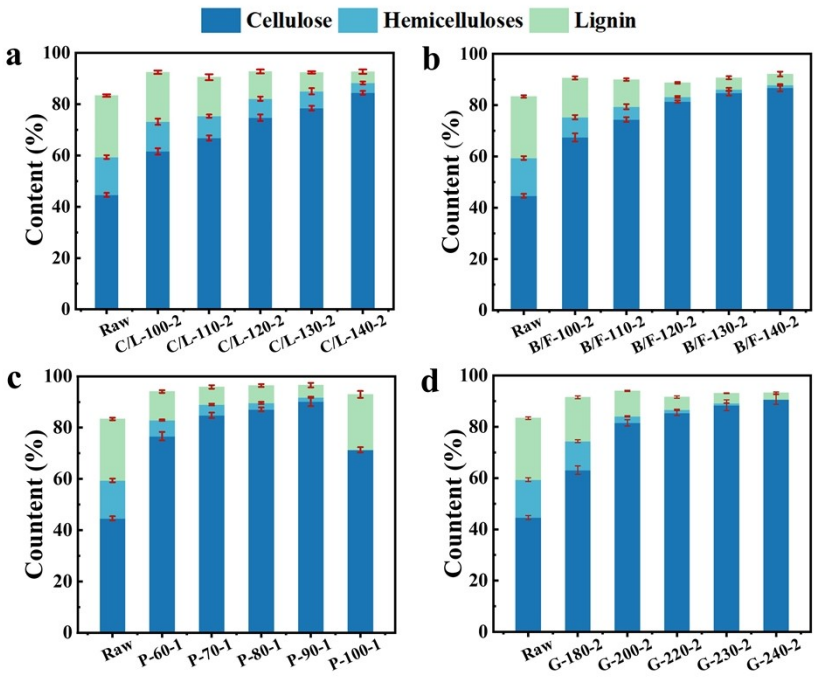

Fig. S4. Chemical composition of pulps produced by different cooking systems. (a) ChCl/LA system. (b) BTEAC/FA system. (c) *p*-TsOH/water system. (d) GVL/water system.

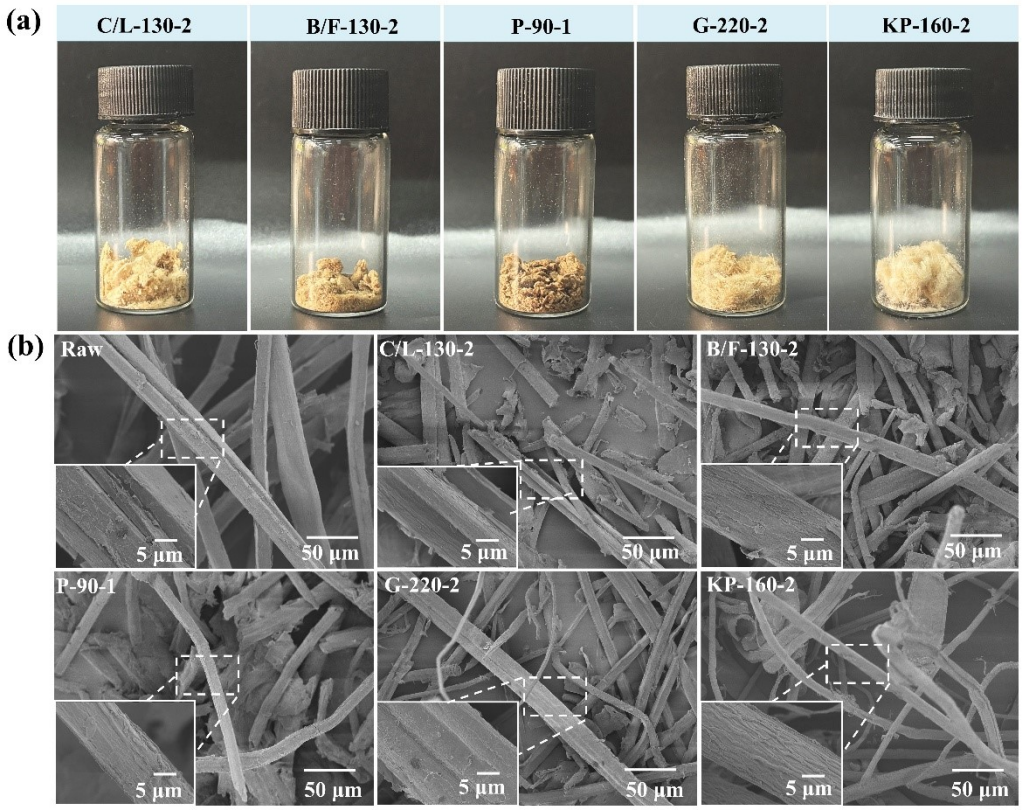

Fig. S5. Morphology of pulp obtained under the optimal pulping conditions of different pulping systems. (a) Visual image. (b) SEM images.

As shown in **Fig. S4a†**, the brightness of pulps differed markedly across systems. P-90-1 had the lowest brightness, likely due to condensed lignin and chromophore formation in strong acid media. C/L-130-2, G-220-2, and KP-160-2 showed higher brightness, with KP-160-2 being the lightest due to its effective degradation of chromophoric groups under alkaline conditions. B/F-130-2 exhibited intermediate brightness, indicating moderate chromophore content and efficient delignification. SEM images **(Fig. S4b†)** revealed that pulping disrupted the original smooth surfaces of bamboo fibers, exposing fibrillar textures. KP-160-2 and B/F-130-2 had rougher, more textured surfaces, suggesting more thorough removal of lignin and hemicelluloses. In contrast, P-90-1 and G-220-2 retained smoother surfaces, indicating incomplete delignification or lignin re-deposition. Fiber shortening was observed for

all pulps, but KP-160-2 maintained relatively longer fibers, likely due to less structural damage during alkaline cooking.

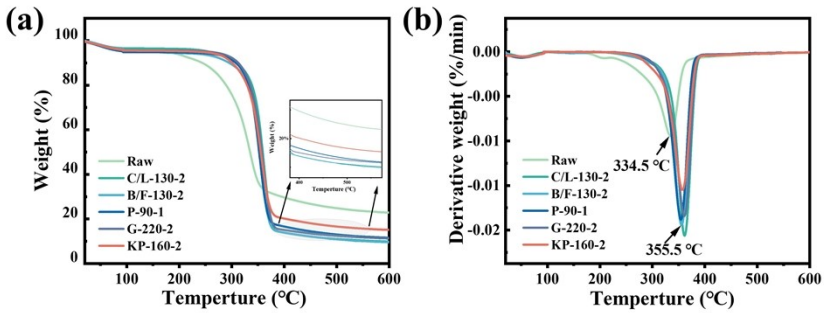

Fig. S6. (a) TGA curves and (b) DTG curves of pulps obtained from different pulping systems.

As shown in the TG and DTG curves **(Fig. S5†)**, three distinct thermal degradation stages are identified: moisture loss (30 to 100 °C), decomposition of cellulose, hemicelluloses, and lignin (100 to 380 °C), and carbonization (380 to 600 °C), involving glycosidic bond cleavage and the formation of volatile fragments.[57] All pulps exhibited improved thermal stability compared to raw bamboo, with maximum degradation temperatures shifting from 334.5 °C to 355.5 °C after pulping. This enhancement is primarily attributed to the removal of thermally labile hemicellulose, extractives, and partial lignin, leading to a more thermally stable cellulose-rich matrix.[58] Final residual masses at 600 °C followed the trend: raw (22.8%) > KP-160-2 (15.1%) > P-90-1 (11.6%) > G-220-2 (11.3%) > C/L-130-2 (9.9%) > B/F-130-2 (9.6%). The low residue of B/F-130-2 reflects its low ash content and high organic purity.

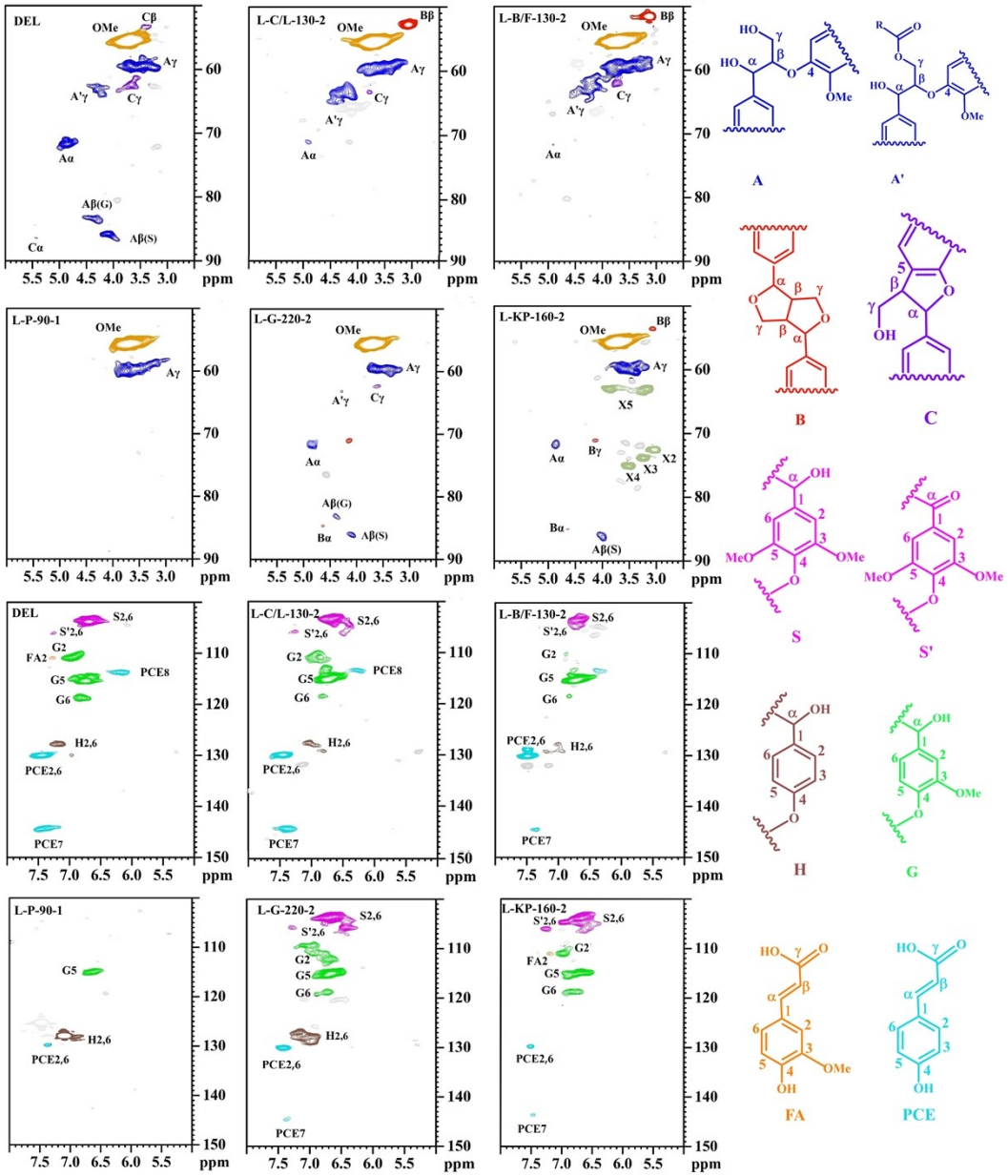

Fig. S7. Side-chain region and aromatic region in the 2D-HSQC NMR of the lignin obtained under optimal cooking conditions of different pulping systems.

Effective utilization of lignin, a major by-product of pulping, is crucial for enhancing the overall efficiency and value of the pulping process. To evaluate structural features and purity, lignins obtained under optimal pulping conditions were compared with native double enzymatic lignin (DEL) using 2D-HSQC NMR spectroscopy **(Fig. S7†)**. Prominent cross-signals corresponding to the xylan backbone (X2, X3, X4, X5)

were observed in L-KP-160-2, indicating significant residual carbohydrate contamination.[17] In contrast, L-B/F-130-2 exhibited minimal non-lignin signals, reflecting higher purity consistent with purity analysis **(Table S11†)**. Compared with DEL. In contrast, the *β-O*-4 signals (Aα, Aβ) were markedly diminished or absent in L-B/F-130-2 and L-C/L-130-2, indicating extensive ether bond cleavage during DES pulping. The weakened β-*O*-4 signal intensity in DES lignins compared to L-KP-160-2 indicated extensive ether bond cleavage, which promoted lignin depolymerization and facilitates extraction from bamboo. The 2D-HSQC spectra of regenerated lignin showed that in the aromatic region, L-G-130-2 and L-KP-160-2 exhibited intensified condensed S-unit signals, indicating a higher degree of condensation, while L-B/F-130-2 displayed weak condensation. Additionally, the disappearance of G2 and G6 signals in L-P-90-1 indicates demethoxylation and aromatic ring condensation.

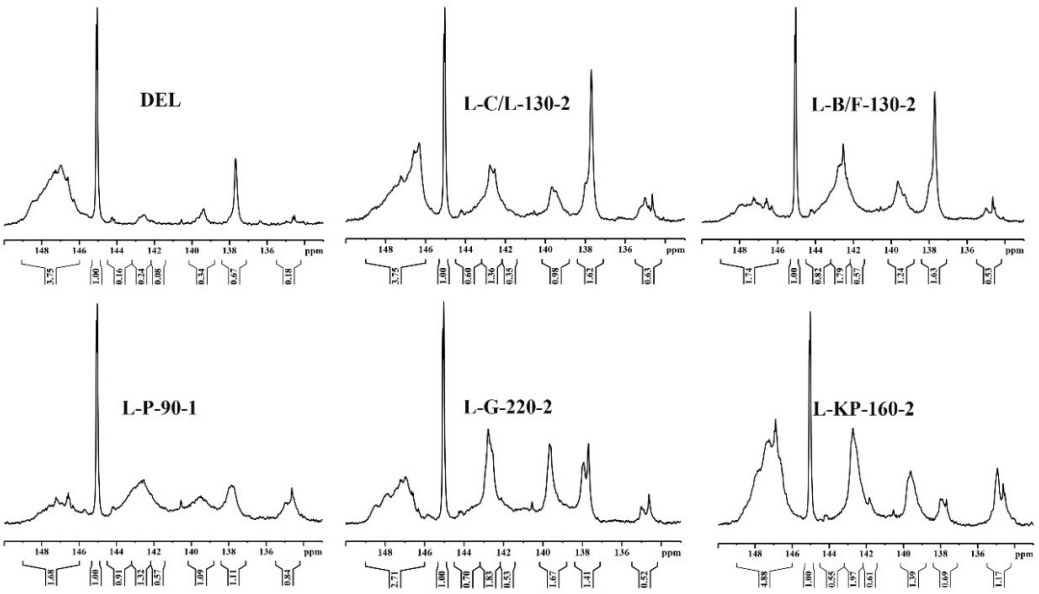

Fig. S8. Quantitative ^{31}P NMR spectra of DEL and lignin obtained under optimal cooking conditions of different pulping systems.

To better understand the chemical reactivity of lignin obtained under optimal pulping conditions, a detailed structural analysis was conducted using ^{31}P NMR technology **(Fig. 6a, Fig. S8† and Table S13†)**. The results show that the content of fatty hydroxyl groups in the lignin separated after cooking is low, ranging from 0.94 to 2.64 mmol/g lignin, which is significantly lower than that of DEL lignin (4.06 mmol/g lignin). This indicates that the aliphatic OH in the lignin components is modified during the cooking process. It is worth noting that the fatty hydroxyl content of L-B/F-130-2 is 0.94 mmol/g lignin and the total phenolic hydroxyl content is as high as 3.28 mmol/g lignin, which may be due to the different degrees of cleavage of β-*O*-4 bonds, while the fatty hydroxyl content of L-KP-160-2 is 2.64 mmol/g lignin and the total phenolic hydroxyl content is 2.82 mmol/g lignin. The increased phenolic hydroxyl content enhances lignin's solubility in green solvents and improves its reactivity, antioxidant capacity, and compatibility with polymers,[59] thereby facilitating its high-value utilization as an amphiphilic biopolymer.

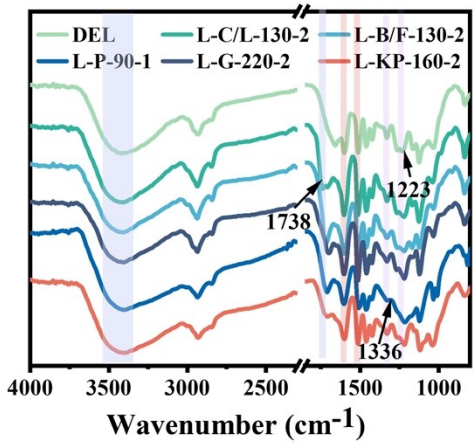

Fig. S9. FT-IR spectrum of lignin obtained under optimal cooking conditions of different pulping systems.

FTIR spectra confirmed that all regenerated lignin samples retained the aromatic backbone, as evidenced by characteristic benzene ring vibrations at 1617, 1518, 1463, and 1431 cm^{-1} **(Fig. S9†)**.[60] The band at 1223 cm^{-1}, attributed to C–O, C–C, and C=O stretching in condensed guaiacyl (G) units, was significantly weakened in L-B/F-130-2, indicating cleavage of β-*O*-4 linkages. A peak at 1336 cm^{-1}, associated with syringyl (S) ring breathing and condensed guaiacyl structures, showed lower intensity in L-B/F-130-2 than in L-KP-160-2, suggesting a lower degree of condensation in DES-derived lignin.[61] These findings underscore the superiority of DES systems in producing high-purity, functionally modified lignin with improved solubility and potential for high-value applications.

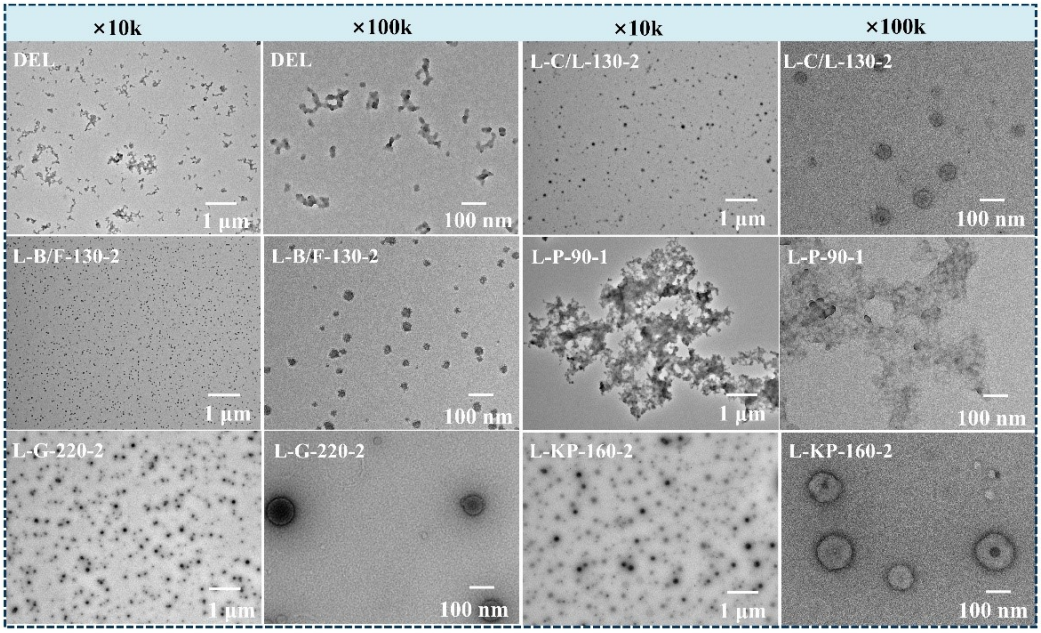

Fig. S10. TEM images of LNPs at different magnifications prepared by acetone rotary evaporation.

TEM analysis **(Fig. 6d, Fig. S10†)** revealed that LNPs from L-C/L-130-2, L-B/F-130-2, and L-G-220-2 were uniformly spherical with particle sizes below 100 nm, whereas DEL and L-P-90-1 formed irregular sheet-like aggregates. L-KP-160-2 also yielded LNPs, but with a larger average diameter (147.35 nm) and sedimentation after 24 h **(Fig. S11b†)**, indicating poor stability. Notably, L-B/F-130-2 produced the smallest and most stable particles (34.89 nm, **Fig. 6d**) with no sedimentation after 24 h **(Fig. S11e†)**. This stability is attributed to mild DES pulping, which increased syringyl unit content and enhanced π–π interactions and hydrogen bonding during self-assembly, as supported by 2D-HSQC and ^{31}P NMR results.[62] Literature and experimental evidence suggest that during antisolvent addition, lignin rapidly aggregates at the organic–water interface **(Fig. S2b)**, where hydrophilic domains interact with water to form the shell and hydrophobic regions assemble into the core.[63] As the water content exceeds that of the organic phase, reverse aggregation may occur, entrapping residual organic solvent within the aggregates. This mechanism accounts for the observed variations in morphology and stability among lignin sources and

underscores the influence of lignin structure and pulping conditions on LNPs performance.[64, 65]

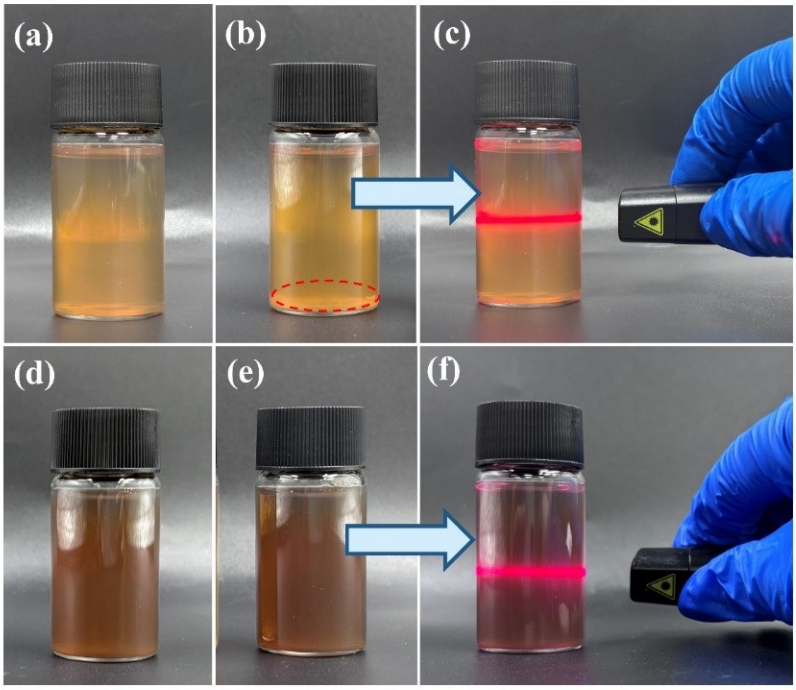

Fig. S11. Photographs of LNPs and its Tyndall were from kraft lignin (L-KP-160-2) and DES lignin (L-B/F-130-2). (a) Image of L-KP-160-2. (b) Image of (a) after 24 h of standing. (c) Tyndall effect of L-KP-160-2. (d) Image of L-B/F-130-2. (e) Image of (d) after 24 h of standing. (f) Tyndall effect of L-B/F-130-2.

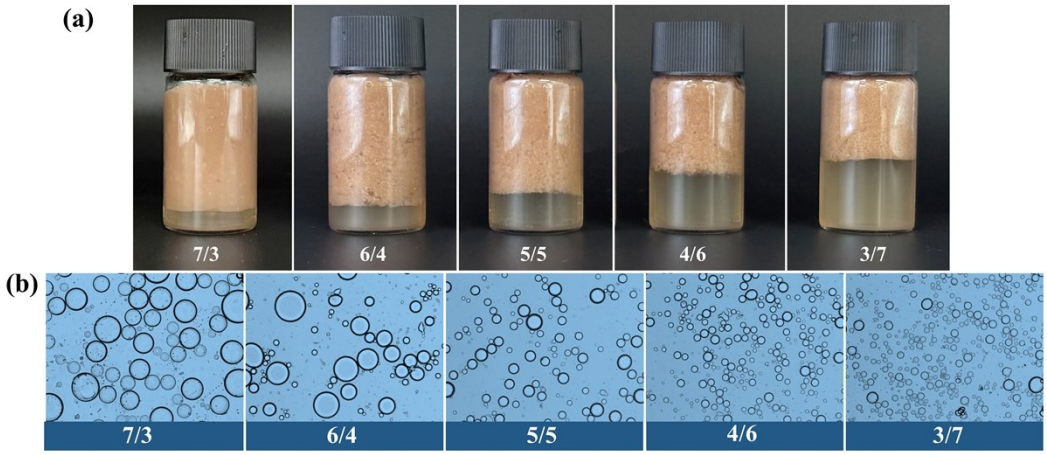

Fig. S12. (a) Photographs of emulsions prepared with different oil-water ratios (from left to right oil/water ratios are 7:3, 6:4, 5:5, 4:6, 3:7). (b) Microscopic image of the corresponding emulsions.

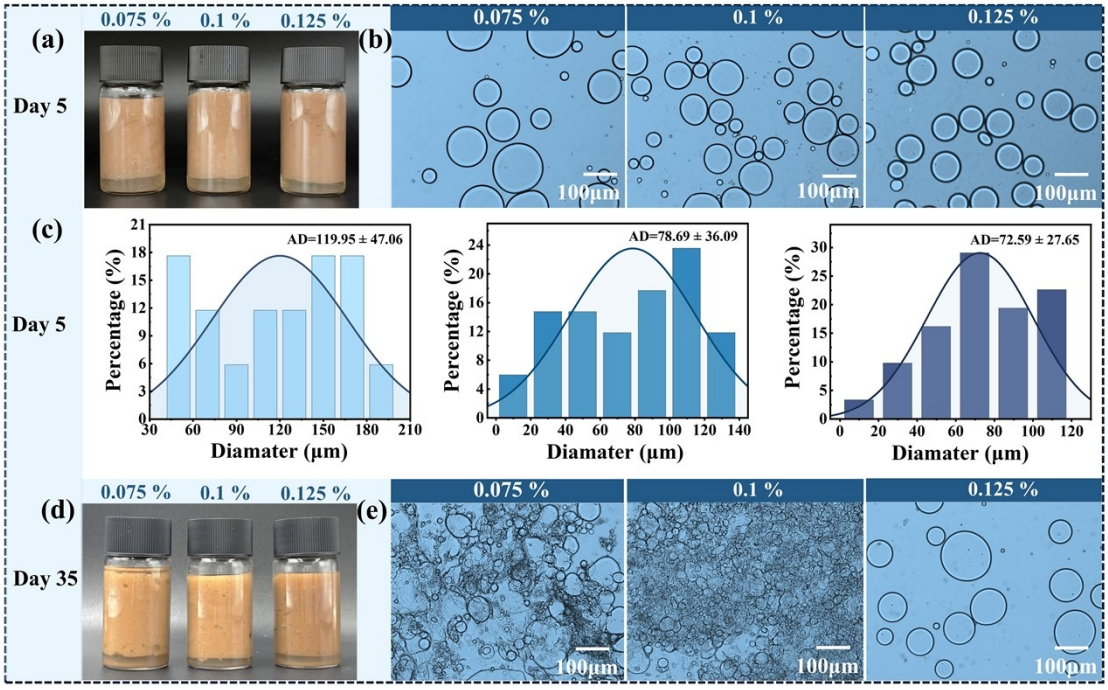

Fig. S13. Lignin nanoparticles are used to stabilize Pickering emulsions. (a) Visual image on day 5. (b) Microscopic image on day 5. (c) Particle-size distribution on day 5. (d) Visual image after 35 days of storage. (e) Microscopic image after 35 days of storage.

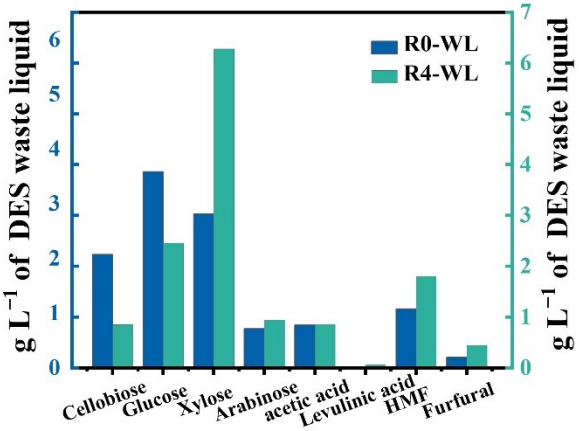

Fig. S14. Content of aqueous phase inhibitors and degradation products in DES waste liquor.

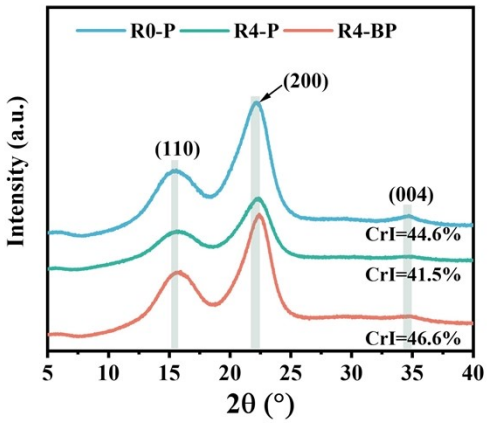

Fig. S15. Comparison of the crystal structure and crystallinity of bleached and unbleached pulps obtained after four DES cycles compared to the initial pulp.

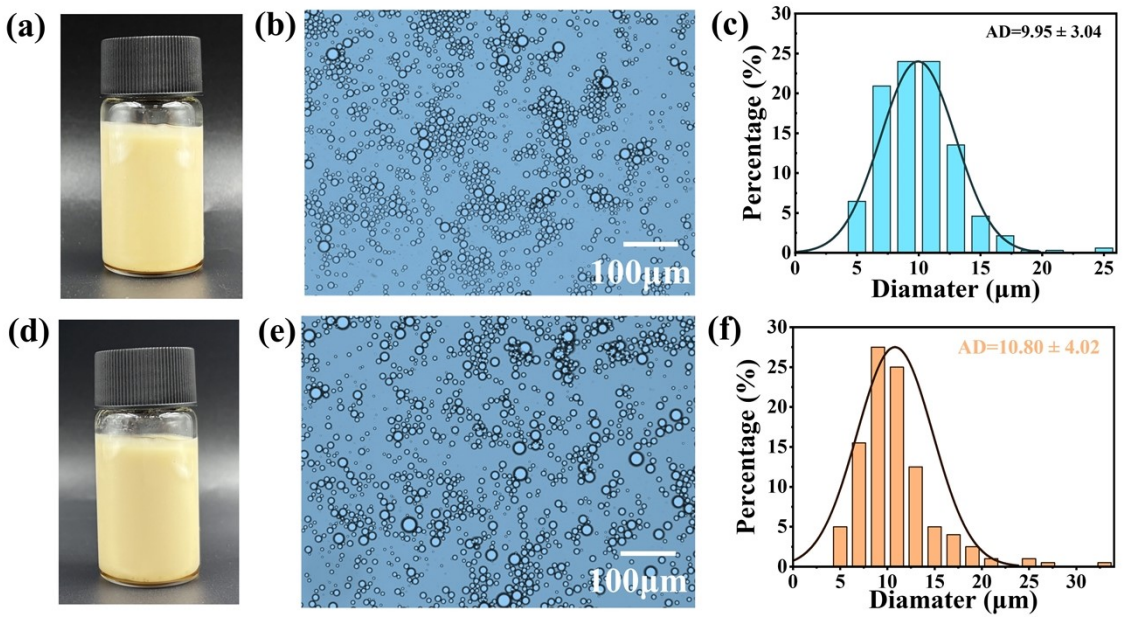

Fig. S16. Pickering emulsions stabilized by lignin nanoparticles prepared after four DES pulping cycles at R-L lignin additions (0.1 wt%). (a) Visual image on day 1. (b) Microscopic image on day 1. (c) Particle-size distribution on day 1. (d) Visual image after 15 days of storage. (e) Microscopic image after 15 days of storage. (f) Particle-size distribution after 15 days of storage.

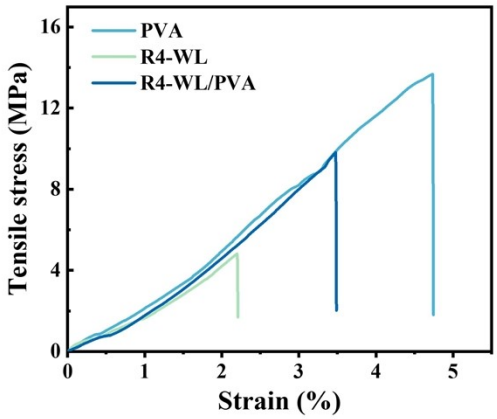

Fig. S17. Stress-strain curves of the prepared adhesives for wood bonding.

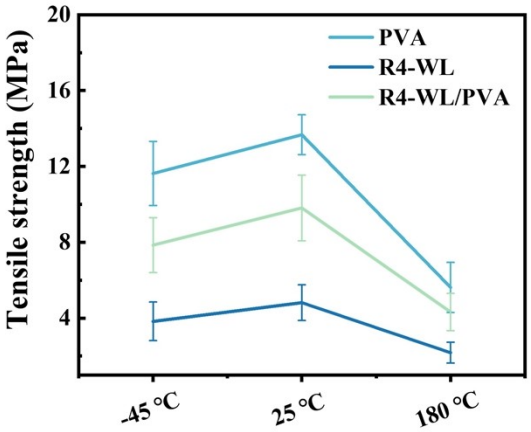

Fig. S18. Mechanical properties of prepared adhesives for wood bonding under extreme conditions.

References

1. M. Wang, D. Yang, Q. Xu, P. Li, C. Yi, Y. Qian and X. Qiu, *Ind. Crops Prod.*, 2021, **162**, 113230.
2. T.-Y. Chen, B. Wang, Y.-Y. Wu, J.-L. Wen, C.-F. Liu, T.-Q. Yuan and R.-C. Sun, *Int. J. Biol. Macromol.*, 2017, **101**, 747–757.
3. A. Sluiter, B. Hames, R. Ruiz, C. Scarlata, J. Sluiter, D. Templeton and D. Crocker, *Laboratory analytical procedure*, 2008, **1617**, 1–16.
4. J. Brand, G. Pecastaings and G. Sèbe, *Carbohydr. Polym.*, 2017, **169**, 189–197.
5. C. Tian, L. Zheng, Q. Miao, C. Nash, C. Cao and Y. Ni, *Tappi J*, 2013, **12**, 21–26.
6. C. Tian, L. Zheng, Q. Miao, C. Cao and Y. Ni, *Cellulose*, 2014, **21**, 3647–3654.
7. L. Segal, J. J. Creely, A. Martin Jr and C. Conrad, *Text. Res. J.*, 1959, **29**, 786–794.
8. Y. Zhou, Y. Cheng, Q. Mi, X. Zhang, J. Zhang and J. Zhang, *Anal. Chem.*, 2022, **94**, 5432–5440.
9. C. Crestini and D. S. Argyropoulos, *J. Agric. Food Chem.*, 1997, **45**, 1212–1219.
10. X.-J. Shen, B. Wang, P.-L. Huang, J.-L. Wen and R.-C. Sun, *Bioresour. Technol.*, 2016, **206**, 57–64.
11. H. Wang, M. L. Maxim, G. Gurau and R. D. Rogers, *Bioresour. Technol.*, 2013, **136**, 739–742.
12. W. N. Association, *URL https://www. world-nuclear. org/information-library/energy-and-the-environment/carbon-dioxide-emissions-from-electricity. aspx*, 2023.
13. X. Liang, J. Wang, Y. Guo, Z. Huang and H. Liu, *Bioresour. Technol.*, 2021, **330**, 124984.
14. X. Liang, Z. Huang, J. Zhang and Y. Guo, *Bioresour. Technol.*, 2023, **384**, 129332.
15. Y. Chen, K. Shen, Z. He, T. Wu, C. Huang, L. Liang and G. Fang, *Cellulose*, 2021, **28**, 11503–11517.
16. Y. Zhang, R. Wu, S. Ni, X. Chen, Z. Wang, Z. Li, Y. Fu, M. Qin and C. Xu, *ChemSusChem*, 2025, e202501445.
17. Z. Zhang, J. Xu, J. Xie, S. Zhu, J. Li, G. Ying and K. Chen, *Green Chem.*, 2023, **25**, 3256–3266.

18. J. Cui, R. Chen, L. Lei and Y. Hou, *Biomass Convers. Biorefin.*, 2024, **14**, 13987–14001.
19. Y. Zhu, L. Li, Y. Hou, C. Xu, G. Hu, Y. Man, V. S. Vladimirovich, J. Li and Q. Xiong, *J. Clean. Prod.*, 2024, **447**, 141652.
20. Y. Xu, Y.-H. Liu, L.-H. Xu, Y.-T. He, J.-L. Wen and T.-Q. Yuan, *Bioresour. Technol.*, 2023, **380**.
21. A. D. Pérez, Y. Roy, C. Rip, S. R. A. Kersten and B. Schuur, *Biomass Convers. Biorefin.*, 2023, **15**, 1377–1391.
22. B. Wang, X. Zhang, J. Li, J. Xu, J. Zeng, M. Li, X. Li and Y. Li, *Int. J. Biol. Macromol.*, 2023, **245**, 125395.
23. S. Shokri, S. Hedjazi, H. Q. Lê, A. Abdulkhani and H. Sixta, *Carbohydr. Polym.*, 2022, **288**, 119364.
24. S. K. Gülsoy, *Ind. Crops Prod.*, 2023, **206**.
25. L. Zhang, J. Chu, S. Gou, Y. Chen, Y. Fan and Z. Wang, *Ind. Crops Prod.*, 2021, **171**.
26. B. Soares, A. M. da Costa Lopes, A. J. Silvestre, P. C. R. Pinto, C. S. Freire and J. A. Coutinho, *Ind. Crops Prod.*, 2021, **160**, 113128.
27. W.-L. Lim, A. A. N. Gunny, F. H. Kasim, I. M. AlNashef and D. Arbain, *Cellulose*, 2019, **26**, 4085–4098.
28. H. Zhao, Z. Gao, M. Wang, X. Li, W. Zheng, D. Li and F. Xu, *Bioresour. Technol.*, 2025, **437**, 133189.
29. C. Tian, C. Duan, Y. Bie, X. Liu, B. Zhou, R. Ma, Q. Fan, Z. Xie and Y. Ni, *Carbohydr. Polym.*, 2025, **348**, 122942.
30. C. Tian, C. Duan, Z. Meng, Y. Wen, X. Feng, Z. Xie and Z. Xie, *Sep. Purif. Technol.*, 2024, **345**, 127358.
31. S. W. Kweon, T. J. Lee, Y. J. Lee, J. H. Seo and H. J. Kim, *Ind. Crops Prod.*, 2025, **235**.
32. A. Kalantari, M. Jonoobi, A. Ashori and P. Moradpour, *J. Polym. Environ.*, 2025, **33**, 400–414.
33. R. Candido and A. Gonçalves, *Carbohydr. Polym.*, 2016, **152**, 679–686.
34. A. M. Das, A. A. Ali and M. P. Hazarika, *Carbohydr. Polym.*, 2014, **112**, 342–349.

35. H. M. Shaikh, A. Anis, A. M. Poulose, S. M. Al-Zahrani, N. A. Madhar, A. Alhamidi, S. H. Aldeligan and F. S. Alsubaie, *Molecules*, 2022, **27**, 1434.
36. J. M. da Silva Neto, C. Oliveira, F. L. da Silva, J. N. Tabosa, J. Pacheco and M. J. da Silva, *BioResources*, 2019, **14**, 3534–3553.
37. R. Battisti, E. Hafemann, C. A. Claumann, R. A. F. Machado and C. Marangoni, *Polym. Eng. Sci.*, 2019, **59**, 891–898.
38. O. A. Hamed, S. Jodeh, N. Al-Hajj, E. M. Hamed, A. Abo-Obeid and Y. Fouad, *J. Wood Sci.*, 2015, **61**, 45–52.
39. N. Mahmood, Z. Yuan, J. Schmidt and C. C. Xu, *Renew. Sust. Energ. Rev.*, 2016, **60**, 317–329.
40. J. Sameni, S. A. Jaffer, J. Tjong and M. Sain, *Curr. Forestry Rep.*, 2020, **6**, 159–171.
41. Y. Yu, W. Cheng, Y. Li, T. Wang, Q. Xia, Y. Liu and H. Yu, *Green Chem.*, 2022, **24**, 3257–3268.
42. G. Akay and C. A. Jordan, *Energ Fuel*, 2011, **25**, 2274–2283.
43. B. H. Suryanto, H.-L. Du, D. Wang, J. Chen, A. N. Simonov and D. R. MacFarlane, *Nat. Catal.*, 2019, **2**, 290–296.
44. J. Baeyens, Q. Kang, L. Appels, R. Dewil, Y. Lv and T. Tan, *Prog. Energy Combust. Sci.*, 2015, **47**, 60–88.
45. J. L. Guil, M. E. Torija, J. J. Giménez, I. Rodríguez-García and A. Giménez, *J. Agric. Food Chem.*, 1996, **44**, 1821–1823.
46. R. S. Costa, B. S. Aranha, A. Ghosh, A. O. Lobo, E. T. da Silva, D. C. Alves and B. C. Viana, *J. Phys. Chem. Solids.*, 2020, **147**, 109678.
47. M. K. Manish Kumar, *Int. J. Pharma Bio Sci.*, 2013, **4**, 337–342.
48. S. K. Mandal and P. C. Banerjee, *Process Biochem.*, 2005, **40**, 1605–1610.
49. Y. Wang, N. Xiao, F. Zhang, Y. He, X. Chen, S. Xie, R. Jing, Y. Sun, C. Jiang and Y. Zhao, *Energy Convers. Manag.*, 2025, **325**, 119359.
50. D. A. Bulushev and J. R. Ross, *ChemSusChem*, 2018, **11**, 821–836.
51. W. Deng, Y. Wang and N. Yan, *Curr. Opin. Green Sustain. Chem.*, 2016, **2**, 54–58.

52. G. Guo and F. Jin, *Biomass Bioenergy*, 2026, **204**, 108470.

53. Y. Chen, Y. Yang, X. Liu, X. Shi, C. Wang, H. Zhong and F. Jin, *Mol. Catal.*, 2023, **545**, 113199.

54. S. Dutta, *Bioresource Technology Reports*, 2025, 102389.

55. Y. Geng, W. Xue, J. Ye, R. Zhang, P. Mishra and J. Zhao, *Green Chem.*, 2025, **27**, 4165–4176.

56. Q. Liu, D. Zhou, Z. Li, W. Luo and C. Guo, *Chin. J. Chem.*, 2017, **35**, 1063–1068.

57. X.-Y. Ye, Y. Chen, J. Yang, H.-Y. Yang, D.-W. Wang, B. B. Xu, J. Ren, D. Sridhar, Z. Guo and Z.-J. Shi, *Adv. Compos. Hybrid Mater.*, 2023, **6**, 106.

58. Y. Chen, X.-Y. Ye, D.-W. Wang, J. Yang, C.-H. Wu, J. Xu, H.-Y. Yang and Z.-J. Shi, *Ind. Crops Prod.*, 2023, **193**, 116248.

59. X.-Y. Hui, C. Zuo, Y. Xu, B. Wang, J.-L. Wen and T.-Q. Yuan, *Chem. Eng. J.*, 2024, **493**, 152517.

60. F. H. Sosa, D. O. Abranches, A. M. da Costa Lopes, J. A. Coutinho and M. C. da Costa, *ACS Sustainable Chem. Eng.*, 2020, **8**, 18577–18589.

61. R. Prado, X. Erdocia, G. F. De Gregorio, J. Labidi and T. Welton, *ACS Sustainable Chem. Eng.*, 2016, **4**, 5277–5288.

62. M. Ma, L. Dai, J. Xu, Z. Liu and Y. Ni, *Green Chem.*, 2020, **22**, 2011–2017.

63. Y. Qian, Y. Deng, X. Qiu, H. Li and D. Yang, *Green Chem.*, 2014, **16**, 2156–2163.

64. Y. Li, X. Qiu, Y. Qian, W. Xiong and D. Yang, *Chem. Eng. J.*, 2017, **327**, 1176–1183.

65. C. H. M. Camargos and C. A. Rezende, *Int. J. Biol. Macromol.*, 2021, **193**, 647–660.